Coupled Systems Mechanics, *Vol. 14, No. 1 (2025) 1-19*
https://doi.org/10.12989/csm.2025.14.1.001

Nonlinear frequency and dynamic response of PLA polymeric imperfect FG sandwich plates under hygrothermal conditions

Zuhair Farhan Abo Alhous[1], Muhsin J. Jweeg[2], Emad Kadum Njim*[3], Ahmed Mouthanna[4], Mujtaba A. Flayyih[5], Royal Madan[6a], Pallavi Khobragade[7] and Praveen Kumar Rai[8]

[1]Department of Mechanical Engineering, Faculty of Engineering, Kufa University, Iraq
[2]College of Technical Engineering, Al-Farahidi University, Iraq
[3]Ministry of Industry and Minerals, State Company for Rubber and Tires Industries, Iraq
[4]College of Engineering, University of Anbar, Ramadi, Anbar, Iraq
[5]Prosthetics and Orthotics Engineering, College of Engineering, AL-Mustaqbal University, 51001 Hillah, Babil, Iraq
[6]Department of Mechanical Engineering, Graphic Era (Deemed to be University), Dehradun 248002, Uttarakhand, India
[7]Department of Civil Engineering, Dev Bhoomi Uttarakhand University, Dehradun, India
[8]Department of Mechanical Engineering, University of Lucknow, Lucknow, Uttar Pradesh, 226007, India

(Received September 27, 2024, Revised January 15, 2025, Accepted January 17, 2025)

Abstract. This paper investigates the nonlinear free vibration behavior of porous functionally graded (PFG) sandwich plates under hygrothermal conditions. The material properties of the PFG plates are assumed to change continuously across the thickness governed by the volume fraction of composition. An enhanced rule of mixtures including the distribution of porosity throughout the cross-section was utilized for material modeling. The foundation medium is modeled as nonlinear, homogeneous, and isotropic, which is then solved by using Galerkin's model. The study employs first-order shear deformation theory (FSDT) in the kinematic relations, and the equations of motion are derived using Hamilton's principle. An analytical solution is developed for the PFG sandwich plates, assuming supported boundary conditions. The study thoroughly examines the fundamental natural frequency of PFG plates, considering the impacts of the hygrothermal environment, porosity volume percentage, and span-to-depth ratio. To validate the analytical results, a numerical analysis using finite element method (FEM) is performed using ANSYS software. A maximum discrepancy of 11% was found between the two approaches.

Keywords: analytical modeling; functionally graded composites; nonlinear free oscillations; porous materials; sandwich structures

1. Introduction

Functionally graded materials (FGMs) have become extensively used across various industries

*Corresponding author, Professor, E-mail: emad.njim@gmail.com
[a]Ph.D., E-mail: royalmadan.me@geu.ac.in

http://www.techno-press.org/?journal=csm&subpage=8 ISSN: 2234-2184 (Print), 2234-2192 (Online)

such as aerospace, nuclear energy, automotive, civil engineering, biomechanics, mechanical engineering, electronics, chemical processing, and shipbuilding, serving as a modern alternative to conventional materials. Since their inception in the 1980s, FGMs have been designed, developed, and successfully implemented in numerous industrial applications (Avcar 2019, Garg *et al.* 2021, Tayeb *et al.* 2024, Zohra *et al.* 2024, Zouatnia *et al.* 2024). These materials are microscopically homogeneous and are composed of two distinct materials, typically a combination of ceramic and metal. Numerous comprehensive studies have been conducted on FGM sandwich structures, exploring their types, fabrication methods, and both static and dynamic behaviors (E.K. Njim *et al.* 2021, Emad Kadum Njim *et al.* 2022, Zaidan and Hasan 2022). Polymer matrix composites are widely used in high-performance applications due to their exceptional mechanical properties. However, apart from mechanical, thermal and magneto-electric loads (Rubine *et al.* 2024), these materials can be subjected to hygro-thermal loading which will cause hygro-thermal stresses that can alter their performance.

On a sandwich plate, vibration analysis was performed for simply supported boundary conditions under a hygro-thermal environment by employing Hamilton's principle (Zenkour and El-Shahrany 2020). Moreover, the dynamic instability of cylindrical shells under hygro-thermal loading was performed using the Rayleigh-Ritz method (Tang and Dai 2021a). A non-linear vibration analysis of carbon nanotube-reinforced composites (CNTRCs) plate under hygro-thermal conditions was performed for different CNT distributions using Galerkin's method (Tang and Dai 2021b). Bending analysis of solid and circular plates has been performed using the differential quadrature method (DQM). The plate was made of an aluminum-based metal matrix in which graphene platelets were reinforced uniformly, various loading namely thermal and humid conditions were considered and solved for different boundary conditions (Sobhy 2021). A stability analysis on a spherical shell made of carbon fiber-reinforced polymer (CFRP) under hygro-thermal impacts was carried out using Galerkin's method (Tang and Dai 2021c). Non-linear hygro-thermal vibration and buckling analysis of porous functionally graded carbon nanotube-reinforced composite (FG-CNTRC) cylindrical panels was carried out analytically (Foroutan *et al.* 2021a). The analysis was extended for sandwich cylindrical structures where the core was surrounded by nonlinear viscoelastic foundations (Foroutan *et al.* 2021b).

The vibration analysis of a laminated composite rectangular plate with four actuating magneto-strictive layers was studied by Hamilton's principle. They found that increasing the actuating layers could dampen the vibrations, also the position of these layers has an impact on dynamic performance (Zenkour and El-Shahrany 2021). In another study, buckling analysis of sandwich plates using higher-order shear deformation theory was carried out (Zaitoun *et al.* 2022). Hygro-thermal stresses were analyzed in a rotating FG cylindrical shell for an auxetic honeycomb core. The sandwich FG faces are composed of graphene (GPL) and metal, for this a parametric study for varying GPL composition, angular velocity, and geometrical parameters was performed using the energy method (Allam *et al.* 2022). In another study, analyzed the hygrometric stress for multilayered sandwich plates and shells by using the 3D shell theory (Brischetto and Torre 2022). Static and dynamic analysis of laminated sandwich plates was conducted for both steady state and transient temperature change. The composite plate is under a hygro-thermal environment and the problem was solved using non-uniform rational B-splines (Gupta *et al.* 2022). By utilizing higher-order shear deformation theory and Hamilton's principle a wave propagation analysis was performed in a sandwich plate with graphite-filled viscoelastic layers (Hua *et al.* 2022). For composite laminated plates, vibration analysis was performed for periodic load under a hygrothermal environment (Karimiasl and Alibeigloo 2022). Further, the impact of temperature and humidity on the stresses induced in a shell was carried out in (Monge *et al.* 2022), and for functionally graded nanobeams buckling analysis was performed under hygro-thermo-mechanical loadings (Wang *et al.* 2022).

Recent studies have also examined the long-term durability of composite materials under severe environmental pressures. In (Zhao *et al.* 2022), compared various porosity distributions and dispersion patterns to examine the impact of hygrothermal stress on shallow shells supported by graphene platelets embedded with shape memory alloy wires. Similarly, under cyclic environmental loads, the performance and durability of interference-fit composite joints were analyzed (Hu *et al.* 2022). In (He *et al.* 2022), studied the low-intensity behavior of spiral shallow shells with porous microsphere coverings in hygrothermal environments, while (Parhi *et al.* 2021) used displacement-type finite element analysis to numerically examine the variational eigen feedback of cylindrical composite shells subjected to multiple delamination. A novel four-variable shear deformation plate model was proposed to analyze the buckling dynamics of FG composite sandwich plates in hydrothermal environments, supported by Winkler-Pasternak elastic foundations (Hellal *et al.* 2021). The natural frequencies of functionally graded plates with piezo-magneto-electro-elastic layers resting on a Pasternak elastic foundation, focusing on the effects of thermo-humidity conditions was studied (Kiarasi *et al.* 2022). Furthermore, the influence of Winkler-Pasternak elastic foundations on the natural frequencies of imperfect functionally graded sandwich beams is investigated numerically (Avcar *et al.* 2022). Recently, the free vibration behavior of functionally graded nanobeams with porosity, along with a consideration of nonlocal parameters and an analysis of high-frequency behavior, has been explored using nonlocal simple higher-order shear deformation theory (Ghazwani *et al.* 2024). Additionally, the free vibration problem of laminated sandwich plates is explored using the wavelet finite element method, including the influence of the geometric and material properties and end conditions on the natural frequency characteristics (Sabherwal *et al.* 2024).

While extensive research has been conducted on the behavior of functionally graded (FG) structures, there remains a scarcity of studies specifically addressing the nonlinear free vibration of FG sandwich plates, particularly those considering the influence of humidity and porosity. This gap is evident in the existing literature. Therefore, this study is dedicated to investigating the nonlinear free vibration characteristics of porous functionally graded (PFG) sandwich plates with simply supported boundary conditions. The research thoroughly examines the impact of thermal conditions, porosity levels, and the span-to-depth ratio on the vibration frequencies of these plates.

2. Mathematical formulation of functionally graded sandwich plates

2.1 Preliminary concepts and definitions

Consider an FG sandwich plate with a length L and a rectangular cross-section $b \times h$, where b and h is the width and height of the plate, respectively, as illustrated in Fig. 1. The PFG plate is formed of anisotropic material with smooth qualities that change through the thickness.

2.2 Properties of material

The plate consists of metal and ceramic, with their respective volume fractions denoted by $V_m(z)$ for metal and $V_c(z)$ for ceramic. The distribution of these materials within the plate is

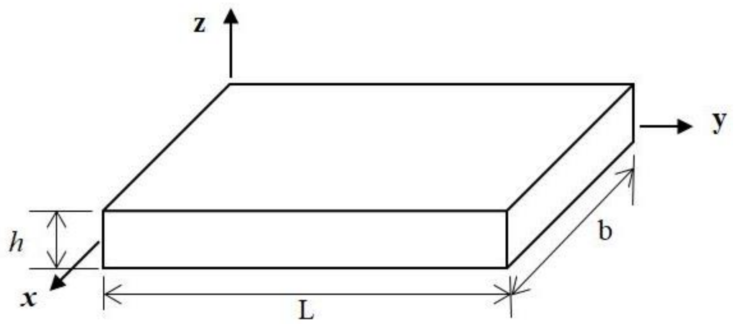

Fig. 1 Geometry and coordinates of FG sandwich plates

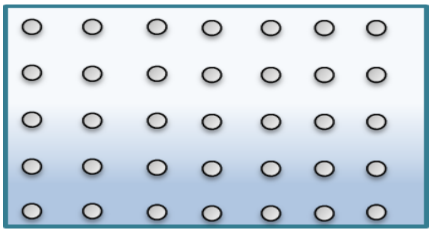

Fig. 2 The Even Porosity distribution for functionally graded plate

described by the following equations (Hadji *et al.* 2022)

$$V_c(z) = \left(\frac{z}{h} + \frac{1}{2}\right)^k, V_m(z) = 1 - V_c(z), \tag{1}$$

In these equations, k is the volume fraction index, which ranges from 0 to ∞. When $k = 0$, the beam is entirely ceramic, whereas $k = \infty$ indicates a completely metal beam. The value of k determines how the materials are distributed within the structure.

The properties of the material across the beam can be expressed as

$$P(z) = (P_c - P_m)\left(\frac{z}{h} + \frac{1}{2}\right)^p + P_m - P_{por} \tag{2}$$

This study assumes an even distribution of porosity, as depicted in Fig. 2, with the specific equations for porosity distribution provided in the subsequent sections.

$$P_{por} = \frac{\beta_p}{2}(P_c + P_m) \tag{3}$$

The mechanical characteristics of the Functionally Graded Material (FGM) exhibit a gradual shift over time across distinct surfaces despite their significant heterogeneity. A simple approach was used to incorporate the effects of porosity given by Eq. (3). To investigate the free and forced vibration of a porous FG plate, a parameter α is introduced that defines the porosity fraction. A porosity fraction determines the amount of porosity distributed in an overall volume. In our study, it is assumed that the porosity is distributed equally in both the phases present. The material properties of the porous material used in this work (PLA) can be illustrated in Table 1. The imperfect (FGM) plate, the thermal expansion, humidity expansion, elastic modulus, and mass density equations can be written as follows (Emad *et al.* 2023, Mouthanna *et al.* 2024)

$$\begin{aligned}\alpha(z) &= \alpha_{\mathrm{m}}(z)\left(1-\beta_p\left(\frac{z}{h}+1\right)^k\right)\\ \beta(z) &= \beta_{\mathrm{m}}(z)\left(1-\beta_p\left(\frac{z}{h}+1\right)^k\right)\\ E(z) &= E_{\mathrm{m}}(z)\left(1-\beta_p\left(\frac{z}{h}+1\right)^k\right)\\ \rho(z) &= \rho_{\mathrm{m}}(z)\left(1-\beta_p\left(\frac{z}{h}+1\right)^k\right)\end{aligned} \tag{4}$$

According to FSDT, the vibration of the plates, is mainly made from FG porous materials. This theory implies that the transverse normal does not stay perpendicular to the mid-surface after the deformation. It assumed that the global displacement field, denoted by left. $(u^{\sim}, v^{\sim}, w^{\sim})$, at any random position within the panel (Hadji and Avcar 2020)

$$\begin{aligned}\tilde{u}(x,y,z,t) &= u(x,y,t) + z\phi_x(x,y,t),\\ \tilde{v}(x,y,z,t) &= v(x,y,t) + z\phi_y(x,y,t),\\ \widetilde{w}(x,y,z,t) &= w(x,y,t),\end{aligned} \tag{5}$$

where (ϕ_x, ϕ_y) illustrate the transverse normal of the slopes around (y) and (x) axes at $(z\ = 0)$. The connections between strain and displacement and the Von Karman nonlinear terms are as follows

$$\begin{gathered}\begin{pmatrix}\varepsilon_x\\ \varepsilon_y\\ \gamma_{xy}\end{pmatrix} = \begin{pmatrix}\varepsilon_x^{\circ}\\ \varepsilon_y^{\circ}\\ \gamma_{xy}^{\circ}\end{pmatrix} + z\begin{pmatrix}\lambda_x\\ \lambda_y\\ \lambda_{xy}\end{pmatrix},\quad \begin{pmatrix}\gamma_{xz}\\ \gamma_{yz}\end{pmatrix} = \begin{pmatrix}\frac{\partial w}{\partial x} + \phi_x\\ \frac{\partial w}{\partial y} + \phi_y\end{pmatrix},\\ \begin{pmatrix}\varepsilon_x^{\circ}\\ \varepsilon_y^{\circ}\\ \gamma_{xy}^{\circ}\end{pmatrix} = \begin{pmatrix}\frac{\partial u}{\partial x} + \frac{1}{2}\left(\frac{\partial w}{\partial x}\right)^2\\ \frac{\partial v}{\partial y} + \frac{1}{2}\left(\frac{\partial w}{\partial x}\right)^2\\ \frac{\partial u}{\partial y} + \frac{\partial v}{\partial x} + \frac{\partial w}{\partial x}\frac{\partial w}{\partial y}\end{pmatrix}, \begin{pmatrix}\lambda_x\\ \lambda_y\\ \lambda_{xy}\end{pmatrix} = \begin{pmatrix}\frac{\partial \phi_x}{\partial x}\\ \frac{\partial \phi_y}{\partial y}\\ \frac{\partial \phi_x}{\partial y} + \frac{\partial \phi_y}{\partial x}\end{pmatrix}\end{gathered} \tag{6}$$

where $(\gamma_{xz}, \gamma_{yz})$ illustrate the components of transverse shear strains in the planes. (xz, yz). Based on Hooke's law, the nonlinear strain-stress relations for a plate may be stated as follows (Ali and Hasan 2022).

$$\begin{gathered}\begin{bmatrix}\sigma_x\\ \sigma_y\\ \tau_{xy}\\ \tau_{yz}\\ \tau_{xz}\end{bmatrix} = \begin{pmatrix}C_{11} & C_{12} & 0 & 0 & 0\\ C_{12} & C_{22} & 0 & 0 & 0\\ 0 & 0 & C_{66} & 0 & 0\\ 0 & 0 & 0 & C_{44} & 0\\ 0 & 0 & 0 & 0 & C_{55}\end{pmatrix}\begin{bmatrix}\epsilon_x - \alpha(z,T)dT - \beta(z,C)dc\\ \epsilon_y - \alpha(z,T)dT - \beta(z,C)dc\\ \gamma_{xy}\\ \gamma_{yz}\\ \gamma_{xz}\end{bmatrix},\\ C_{11}^{(j)} = C_{22}^{(j)} = \frac{E^{(j)}(z)}{1-\nu^2}, C_{12}^{(j)} = \frac{\nu E^{(j)}(z)}{1-\nu^2},\\ C_{44}^{(j)} = C_{55}^{(j)} = C_{66}^{(j)} = K_s\frac{E^{(j)}(z,T)}{2(1+\nu)}\end{gathered} \tag{7}$$

Here, dT=(T-$T0$) and dc=(C-$C0$) increase in both humidity and temperature concentration, respectively, and (α) consists of the coefficient of thermal expansion caused by humidity in the primary material directions. Where (K_s) is the factor used to adjust for shear and is given by $(K_s = 5/6)$. The Governing equations

$$\delta u\!:\frac{\partial N_x}{\partial x}+\frac{\partial N_{xy}}{\partial y}=I_0\frac{\partial^2 u}{\partial t^2}+I_1\frac{\partial^2\phi_x}{\partial t^2},\delta v\!:\frac{\partial N_{xy}}{\partial x}+\frac{\partial N_y}{\partial y}=I_0\frac{\partial^2 v}{\partial t^2}+I_1\frac{\partial^2\phi_y}{\partial t^2},\delta w\!:\frac{\partial Q_x}{\partial x}+\frac{\partial Q_y}{\partial y}+ N_x\frac{\partial^2 w}{\partial x^2}+2N_{xy}\frac{\partial^2 w}{\partial x\partial y}+N_y\frac{\partial^2 w}{\partial y^2}+q=I_0\frac{\partial^2 w}{\partial t^2}$$
$$\delta Q_x\!:\frac{\partial M_x}{\partial x}+\frac{\partial M_{xy}}{\partial y}-Q_x=I_2\frac{\partial^2\phi_x}{\partial t^2}+I_1\frac{\partial^2 u}{\partial t^2},\delta Q_y\!:\frac{\partial M_{xy}}{\partial x}+\frac{\partial M_y}{\partial y}-Q_y=I_2\frac{\partial^2\phi_y}{\partial t^2}+I_1\frac{\partial^2 v}{\partial t^2} \tag{8}$$

where

$$\begin{gathered}N_x=\int_{-\frac{h}{2}}^{\frac{h}{2}}\sigma_x\,dz+\Phi_1,N_y=\int_{-\frac{h}{2}}^{\frac{h}{2}}\sigma_y\,dz+\Phi_1,N_{xy}=\int_{-\frac{h}{2}}^{\frac{h}{2}}\sigma_{xy}dz,\\ M_x=\int_{-\frac{h}{2}}^{\frac{h}{2}}\sigma_x\,zdz+\Phi_2,\ M_y=\int_{-\frac{h}{2}}^{\frac{h}{2}}\sigma_y\,zdz+\Phi_2,\\ M_{xy}=\int_{-\frac{h}{2}}^{\frac{h}{2}}\sigma_{xy}z\,dz\big(Q_x,Q_y\big)=\int_{-\frac{h}{2}}^{\frac{h}{2}}\big(\sigma_{xz},\sigma_{yz}\big)\,dz,\\ \Phi_1=-\frac{1}{1-\upsilon}\int_{-\frac{h}{2}}^{\frac{h}{2}}E(z,T)\,(\alpha(z,T)dT+\beta(z,C)dc)dz,\\ \Phi_2=-\frac{1}{1-\upsilon}\int_{-\frac{h}{2}}^{\frac{h}{2}}E(z,T)\,(\alpha(z,T)dT+\beta(z,C)dc)z.\,dz.\end{gathered} \tag{9}$$

The symbols can denote the force resultants of a plate (N_x,N_y,N_{xy}), while the moment resultants can be represented by the symbols (M_x,M_y,M_{xy}), and the transverse force resultants can be denoted by (Q_x,Q_y). When Eq. (7) is placed into Eq. (10) taking Eq. (6) into consideration, the following results are obtained

$$N_x=I_{10}\varepsilon_x^\circ+I_{20}\varepsilon_y^\circ+I_{11}\frac{\partial\phi_x}{\partial x}+I_{21}\frac{\partial\phi_y}{\partial y}+\Phi_1,\quad N_y=I_{20}\varepsilon_x^\circ+I_{10}\varepsilon_y^\circ+I_{21}\frac{\partial\phi_x}{\partial x}+I_{11}\frac{\partial\phi_y}{\partial y}+ \Phi_1,\quad N_{xy}=I_{30}\gamma_{xy}^\circ+2I_{31}\left(\frac{\partial\phi_x}{\partial y}+\frac{\partial\phi_y}{\partial x}\right),$$
$$M_x=I_{11}\varepsilon_x^\circ+I_{21}\varepsilon_y^\circ+I_{12}\frac{\partial\phi_x}{\partial x}+I_{22}\frac{\partial\phi_y}{\partial y}+\Phi_2,\ M_y=I_{21}\varepsilon_x^\circ+I_{11}\varepsilon_y^\circ+I_{22}\frac{\partial\phi_x}{\partial x}+I_{12}\frac{\partial\phi_y}{\partial y}+ \Phi_2,\ M_{xy}=I_{31}\gamma_{xy}^\circ+I_{32}\left(\frac{\partial\phi_x}{\partial y}+\frac{\partial\phi_y}{\partial x}\right),Q_x=K_sI_{30}\gamma_{xz},Q_y=K_sI_{30}\gamma_{yz}, \tag{10}$$

3. Analytical solution

The analytical solutions (Navier-type) are derived for the analysis of free-vibration of PFG plates under hygrothermal conditions. The end conditions of the (FGM) thin plate are simply supported and subjected to the uniform pressure. For the boundary condition considered, it can be written as

$$w=N_{xy}=\phi_y=0,N_x=N_{x0},atx=0,a,w=N_{xy}=\phi_x=0,N_y=N_{y0},aty=0,b, \tag{11}$$

The mode shape is stated as follows because it has to meet the constraints that are provided in Eq. (11)

$$w(x,y,t)=W(t)\,sin\,\lambda_m\,x\,sin\,\delta_n\,y,\phi_x(x,y,t)=\Phi_x(t)\,cos\,\lambda_m\,x\,sin\,\delta_n\,y,\phi_y(x,y,t)\ =\ \Phi_y(t)\,sin\,\lambda_m\,x\,cos\,\delta_n\,y \tag{12}$$

Plug (12) into (13) to get the stress function coefficients

$$\begin{pmatrix} A_{11}\frac{\partial^4 f}{\partial x^4}+A_{22}\frac{\partial^4 f}{\partial y^4}+(A_{66}-2A_{12})\frac{\partial^4 f}{\partial x^2\partial y^2}-B_{21}\frac{\partial^3\phi_x}{\partial x^3}-B_{12}\frac{\partial^3\phi_y}{\partial y^3} \\ +(B_{66}-B_{11})\frac{\partial^3\phi_x}{\partial x\partial y^2}+(B_{66}-B_{22})\frac{\partial^3\phi_y}{\partial x^2\partial y}-\left(\frac{\partial^2 w^2}{\partial x\partial y}-\frac{\partial^2 w}{\partial x^2}\frac{\partial^2 w}{\partial y^2}\right)\end{pmatrix}=0 \tag{13}$$

$$\tilde{f}(x,y,t)=\begin{pmatrix} \tilde{A}_1(t)\cos 2\lambda_m x+\tilde{A}_2(t)\cos 2\delta_n y+ \\ \tilde{A}_3(t)\sin\lambda_m x\sin\delta_n y+\frac{1}{2}N_{x0}y^2+\frac{1}{2}N_{y0}x^2\end{pmatrix} \tag{14}$$

Where

$$\begin{gathered}\tilde{A}_1(t)=\frac{\delta_n^2}{32A_{11}\lambda_m^2}W^2,\delta_1=(-1)^m-1,\delta_2=(-1)^n-1\,, \\ \lambda=\frac{a}{b},\tilde{A}_2(t)=\frac{\lambda_m^2}{32A_{22}\delta_n^2}W^2, \\ \tilde{A}_3(t)=\frac{[B_{21}\lambda_m^3+(B_{11}-B_{66})\lambda_m\delta_n^2]\Phi_x(t)+[\delta_n^3B_{12}+(B_{22}-B_{66})\lambda_m^2\delta_n]\Phi_y(t)}{[A_{11}\lambda_m^4+A_{22}\delta_n^4+(A_{66}-2A_{12})\lambda_m^2\delta_n^2]},\end{gathered} \tag{15}$$

Consider the finite-geometry model of a thin plate with four corners that are simply supported and immobile, exposed to thermal stresses. The circumstances shown by the immovable on the margins are as follows: $u=0$ on $x=0,a$ and $v=0$ on $y=0,b$

$$\int_0^a\int_0^b\frac{\partial u}{\partial x}dxdy=0,\int_0^a\int_0^b\frac{\partial v}{\partial y}dxdy=0 \tag{16}$$

$$\begin{gathered}\frac{\partial u}{\partial x}=A_{22}\frac{\partial^2 f}{\partial y^2}-A_{12}\frac{\partial^2 f}{\partial x^2}-B_{11}\frac{\partial\phi_x}{\partial x}-B_{12}\frac{\partial\phi_y}{\partial y}-\frac{1}{2}\left(\frac{\partial w}{\partial x}\right)^2+C_{11}^*\Phi_1+\Phi_2,\frac{\partial v}{\partial y}=A_{11}\frac{\partial^2 f}{\partial x^2}- \\ A_{12}\frac{\partial^2 f}{\partial y^2}-B_{21}\frac{\partial\phi_x}{\partial x}-B_{22}\frac{\partial\phi_y}{\partial y}-\frac{1}{2}\left(\frac{\partial w}{\partial y}\right)^2+C_{22}^*\Phi_1+\Phi_2\end{gathered} \tag{17}$$

The following expression of N_{x0} and N_{y0} are obtained by inserting Eqs. (12)-(14) into Eq. (17), followed by the results being combined into Eq. (16)

$$\begin{gathered}N_{x0}=\begin{pmatrix} \frac{4\delta_n}{\lambda_m ab}\tilde{A}_3-\frac{4}{\delta_n ab}\frac{(B_{21}A_{12}+A_{11}B_{11})}{H_{11}}\Phi_x-\frac{4}{\lambda_m ab}\frac{(B_{22}A_{12}+A_{11}B_{12})}{H_{11}}\Phi_y- \\ \frac{4}{\delta_n\lambda_m R}\frac{A_{12}}{H_{11}}W+\frac{\delta_n\lambda_m}{8ab}\frac{(\delta_n^2A_{12}+\lambda_m^2A_{11})}{H_{11}}W^2-\frac{(C_{11}^*A_{11}+C_{22}^*A_{12})}{H_{11}}\Phi_1-\frac{(A_{11}+A_{12})}{H_{11}}\Phi_2\end{pmatrix} \\ N_{y0}=\begin{pmatrix} \frac{4\lambda_m}{\delta_n ab}\tilde{A}_3-\frac{4}{\delta_n ab}\frac{(B_{11}A_{12}+A_{11}A_{22}B_{21})}{H_{11}}\Phi_x-\frac{4}{\lambda_m ab}\frac{(B_{12}A_{12}+A_{22}B_{22})}{H_{11}}\Phi_y- \\ \frac{4}{\delta_n\lambda_m R}\frac{A_{22}}{H_{11}}W+\frac{\delta_n\lambda_m}{8ab}\frac{(\lambda_m^2A_{12}+\delta_n^2A_{22})}{H_{11}}W^2-\frac{(C_{11}^*A_{12}+C_{22}^*A_{22})}{H_{11}}\Phi_1-\frac{(A_{12}+A_{22})}{H_{11}}\Phi_2\end{pmatrix}\end{gathered} \tag{18}$$

Solving the above the following form is obtained

$$\begin{gathered}\begin{pmatrix} r_{12}\Phi_x+r_{13}\Phi_y+r_{14}(W)\Phi_x+r_{15}(W)\Phi_y+ \\ r_{16}(W)+r_{17}W^2+r_{19}W^3+H_{32}q\end{pmatrix}=I_0\frac{d^2W}{dt^2} \\ r_{21}W+r_{22}\Phi_x+r_{23}\Phi_y+n_7(W)+n_8W^2=\tilde{\rho}_1\ddot{\Phi}_x, \\ r_{31}W+r_{32}\Phi_x+r_{33}\Phi_y+n_9(W)+n_{10}W^2=\tilde{\rho}_1\ddot{\Phi}_y,\end{gathered} \tag{19}$$

When looking at the equations above, the coefficients should be entered as follows:

Taking into consideration the fact that the FGM plate is being subjected to an evenly distributed transverse load $(q = Qsin\Omega t)$. The generic equation for a nonlinear system then becomes

$$\begin{pmatrix} I_0 \frac{d^2W}{dt^2} - r_{12}\Phi_x - r_{13}\Phi_y - r_{14}(W)\Phi_x - \\ r_{15}(W)\Phi_y - r_{16}(W) - r_{17}W^2 - r_{19}W^3 \end{pmatrix} = H_{32}Q\sin\Omega\,t, r_{21}W + r_{22}\Phi_x + r_{23}\Phi_y + \\ n_7(W) + n_8W^2 = \tilde{\rho}_1\ddot{\Phi}_x, \\ r_{31}W + r_{32}\Phi_x + r_{33}\Phi_y + n_9(W) + n_{10}W^2 = \tilde{\rho}_1\ddot{\Phi}_y, \tag{20}$$

The inertial forces produced by the rotation angles $(\ddot{\Phi}_x, \ddot{\Phi}_y)$ are small, so can be neglected. Thus

$$\Phi_x = z_1W + z_2W^2 \\ z_1 = \left(\frac{r_{23}}{(r_{22}r_{33}-r_{23}r_{32})}r_{31} + \frac{r_{23}}{(r_{22}r_{33}-r_{23}r_{32})}n_9 - \left(\frac{r_{21}r_{33}}{r_{22}r_{33}-r_{23}r_{32}}\right) - \left(\frac{n_7r_{33}}{r_{22}r_{33}-r_{23}r_{32}}\right)\right) \\ z_2 = \left(\left(\frac{r_{23}n_{10}}{r_{22}r_{33}-r_{23}r_{32}}\right) - \left(\frac{n_8r_{33}}{r_{22}r_{33}-r_{23}r_{32}}\right)\right) \tag{21}$$

And

$$\Phi_y = z_3W + z_4W^2 \\ z_3 = -\left(\frac{r_{31}}{r_{33}} + \frac{r_{32}}{r_{33}}z_1 + \frac{n_9}{r_{33}}\right), z_4 = -\left(\frac{r_{32}z_2}{r_{33}} + \frac{n_{10}}{r_{33}}\right) \tag{22}$$

Then, by substituting Eqs. (21) and (22) into Eq. (20), get

$$\begin{pmatrix} I_0\frac{d^2W}{dt^2} - (r_{12}z_1 + r_{13}z_3 + r_{16})W - \\ (r_{12}z_2 + r_{13}z_4 + r_{14}z_1 + r_{15}z_3 + r_{17})W^2 - \\ (r_{14}z_2 + r_{15}z_4 + r_{19})W^3 \end{pmatrix} = H_{32}Q\sin\Omega\,t \tag{23}$$

Now, it is possible to calculate, the nonlinear vibration, the frequency-amplitude relationship, the fundamental frequencies of the (FGM) plate, as well as the nonlinear dynamical responses of the (FGM) plate by using Eq. (22). The nonlinear dynamical responses of an FGM plate may be determined by applying the starting conditions left $(W(0) = 0,\ \dot{W}(0) = 0)$ to Eq. (22), and then solving that equation. The plate in the state of $(q = 0)$, the linear natural frequencies can be derived by solving the equation as

$$\omega = \sqrt{\frac{-(r_{12}z_1 + r_{13}z_3 + r_{16})}{I_0}} \tag{24}$$

4. Numerical solution

To confirm the results of the proposed method, numerical techniques can be utilized, with the Finite Element Analysis (FEA) method being the most precise among them (Raad *et al.* 2024, Madan *et al.* 2024, Abd Alqader *et al.* 2024). In this study, the ANSYS software (Version 2021 R1) is employed to implement the finite element method. A 3D model of the functionally graded (FG) sandwich plate is created, and the appropriate boundary conditions are applied to the plate's sides for modal analysis, as depicted in Fig. 3.

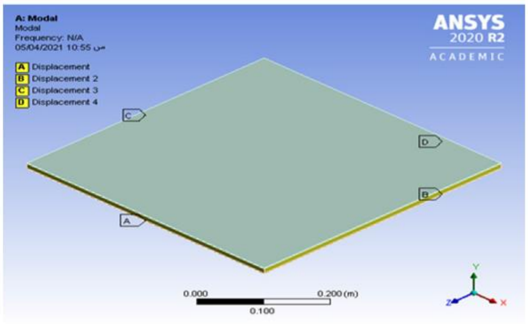

Fig. 3 Simply supported boundary conditions model

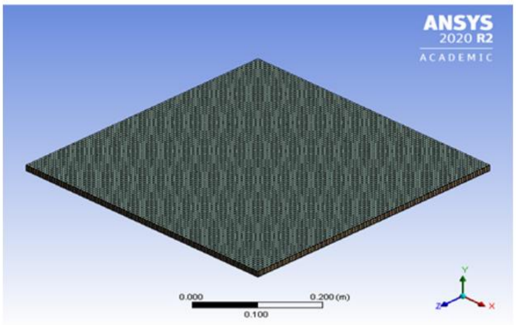

Fig. 4 The meshed model

Table 1 Mechanical and hygrothermal properties of PLA material

Property	Value
Density (G/CM³)	1.24
Poisson's Ratio	0.35
Modulus of elasticity (GPA)	3.5
Thermal expansion coefficient (1/K)	41×10^{-6}
Moisture absorption (WT% H_2O)	5×10^{-4}

The plate dimensions are 0.3×0.3 m with a thickness of 10 mm having porosity distribution through thickness direction. A precise mesh is generated using the 8-node SOLID186 element type, resulting in a total of 40,000 elements, as shown in Fig. 4. The mechanical properties of the FG core are calculated using Eqs. (2) and (3), while the skin layers are treated as isotropic materials, which are then incorporated into the model. Glue conditions are applied at the interfaces of layers and between the layers and the sandwich plate's skin to prevent separation. Modal analysis is then conducted on the selected models to determine the free vibration characteristics, including natural frequencies and mode shapes, based on the previously discussed parameters.

5. Results and discussion

5.1 Effect of porosity parameter

Illustrative examples are given in this step to investigate the impact of porosity on the plate-free vibration characteristic. The PFG plates are assumed to comprise the following materials, as shown in Table 1.

Table 2 includes the results obtained from analytical and numerical solutions on functionally graded polymeric PLA materials, at each of the conditions described, and for all materials where the natural frequency was calculated for each case. The humidity values were varied from (0%, 20%, and 40%), porosity levels (βp=0 to 0.4), power-law index (k=0, 1, 3), and a constant temperature differential (dT=0°C). The analysis shows that the natural frequency decreases with an increase in porosity and humidity levels. It is to be noted that at low levels such as 0% humidity, the variation between the analytical and numerical results is relatively small around

Table 2 Comparison for numerical and analytical natural frequency of (PLA) FGM plate, for dT=0°C

Humidity change (%)	Porosity (%)	Frequency (Hz)		Discrepancy (%)
		Analytical	Numerical	
0	0	246	234	4.878
	20	246	233	5.285
	40	246	237	3.659
	0	246	237	3.659
	20	245	228	6.939
	40	242	229	5.372
	0	246	237	3.659
	20	233	219	6.009
	40	199	181	9.045
20	0	245	230	6.122
	20	244	228	6.557
	40	241	225	6.639
	0	245	227.5	7.143
	20	243	222	8.642
	40	241	218	9.544
	0	245	226	7.755
	20	230	219	4.783
	40	190	177	6.842
40	0	238	224	5.882
	20	242	226	6.612
	40	239	222	7.113
	0	244	218	10.656
	20	241	216	10.373
	40	233	214	8.155
	0	244	219	10.246
	20	222	198	10.811
	40	182	162	10.989

3.7% while increasing it further, the numerical frequencies show a significant drop, with the discrepancy peaking at 10.989%. Additionally, it was observed in Fig. 5, that the natural frequency decreases more noticeably at the 30% and 40% porosity percentages. From the obtained results it is concluded that there are clear shifts in natural frequencies and mode shapes due to temperature and moisture effects. However, the porosity weakens the stiffness of the plate so a lower frequency was obtained as the porosity percentage increased. As demonstrated in the above results, it is extremely difficult to design and analyze FG PLA plates under such conditions and it is therefore imperative to consider material properties, environmental factors, as well as advanced numerical techniques to make accurate predictions.

Based on five types of boundary conditions, Table 3 illustrates how humidity affects the natural frequency of PFG plates. The results show that humidity-induced changes in a plate's natural frequency can be attributed to changes in its material properties, such as reduced stiffness and increased mass. Due to moisture absorption and mechanical constraints, clamped plates usually

Table 3 Numerical solution of the natural frequency (Hz) of plates for different BCs at 20% humidity change

BCs	*k*	Porosity		
		0	0.2	0.4
CCCC	0	306	304.5	301
	1	303.8	300	298.5
	3	298	295	291.5
CCCS	0	273	272.7	270.2
	1	271.95	269.7	266.5
	3	268.4	265	263.5
CSCS	0	258.65	257.5	255.9
	1	257.40	256.25	254.35
	3	255.85	254.78	253.90
SSSS	0	230	228	225.5
	1	227.5	222.4	218
	3	226.3	219.7	177
FCFC	0	161.2	158.6	155.2
	1	154.5	151.8	149.2
	3	150.54	148.80	145.75

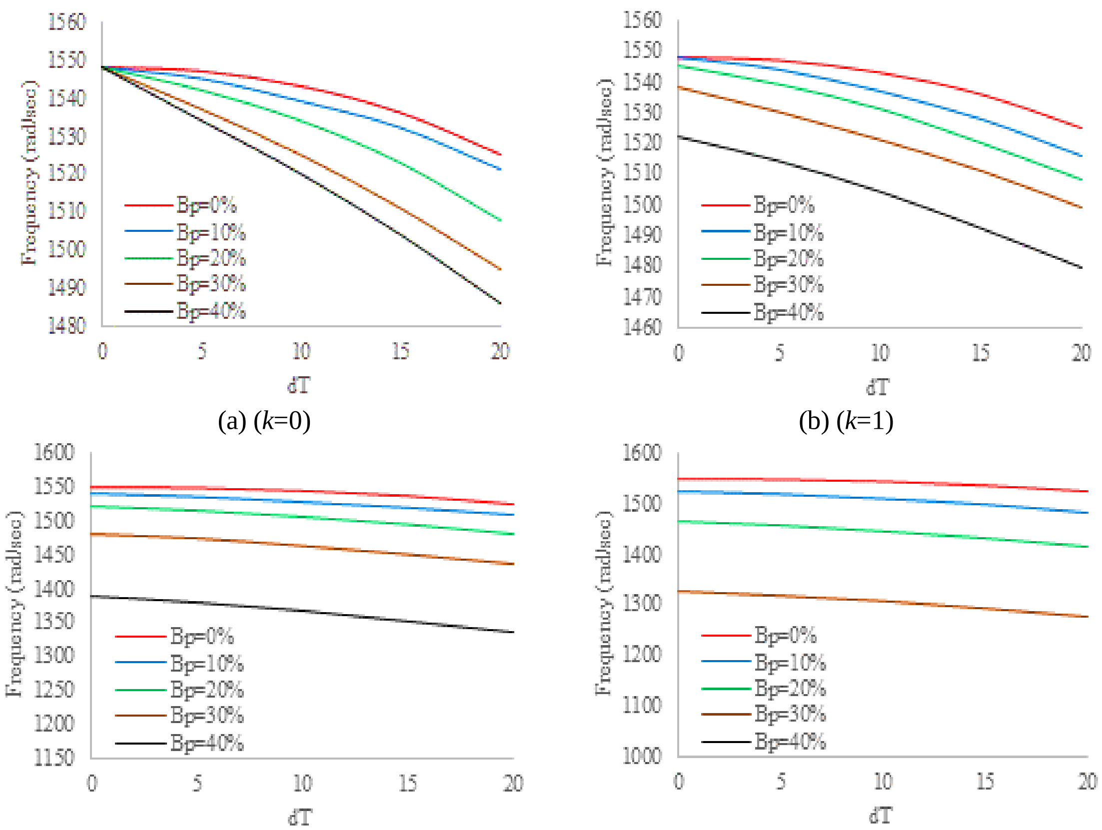

(a) (*k*=0) (b) (*k*=1)

(c) (*k*=2) (d) (*k*=3)

Fig. 5 Results of the natural frequency with various porosity parameters at $dc = 0\%$

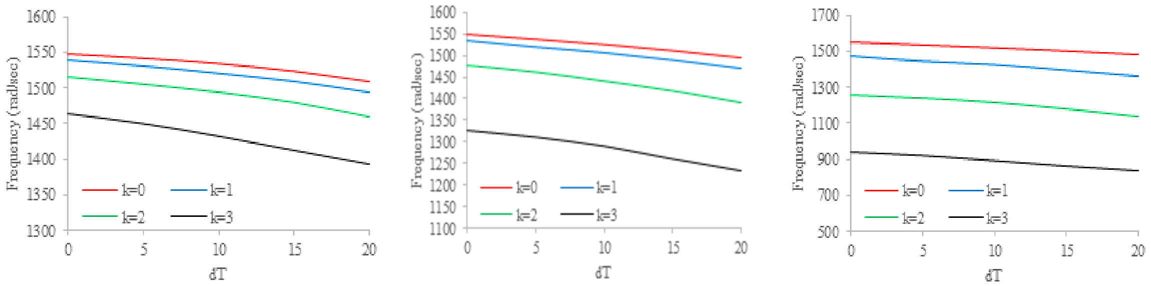

(a) (βp=20%) (b) (βp=30%) (c) (βp=40%)

Fig. 6 The natural frequency of plate with FGM effect, for *dc*=0%

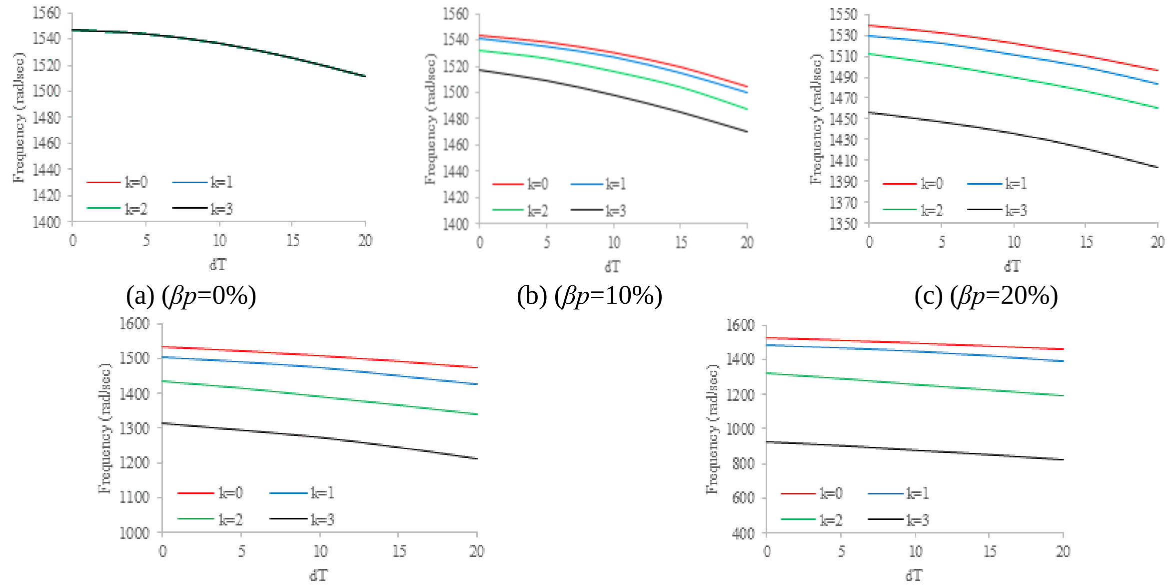

(a) (βp=0%) (b) (βp=10%) (c) (βp=20%)

(d) (βp=30%) (e) (βp=40%)

Fig. 7 Natural frequency of plate with FGM effect, for *dc*=10%

exhibit the most significant decrease in natural frequency compared to the other boundary conditions. However, the mechanical behavior can be complex, depending on the interaction between the moisture content and the material's mechanical properties.

5.2 Effect of functionally gradient index change

In this section, the natural frequency and response of the functionally graded polymeric materials were performed under the influence of the functional gradient change. The effect of the temperature difference with the fixation of the difference with humidity and porosity was calculated and studied. Figs. 6-9 show the results of the analytical solution, for example by considering (βp=0%, *dc*=0%, *k*=0 to 3, *dT*=0 to 20°C), in this case, the humidity difference was fixed at (*dc*=0%) with a porosity (βp=0%). Then, the natural frequency and response of the polymeric materials chosen for the tests were calculated at a functional gradient (*k*=0) with a

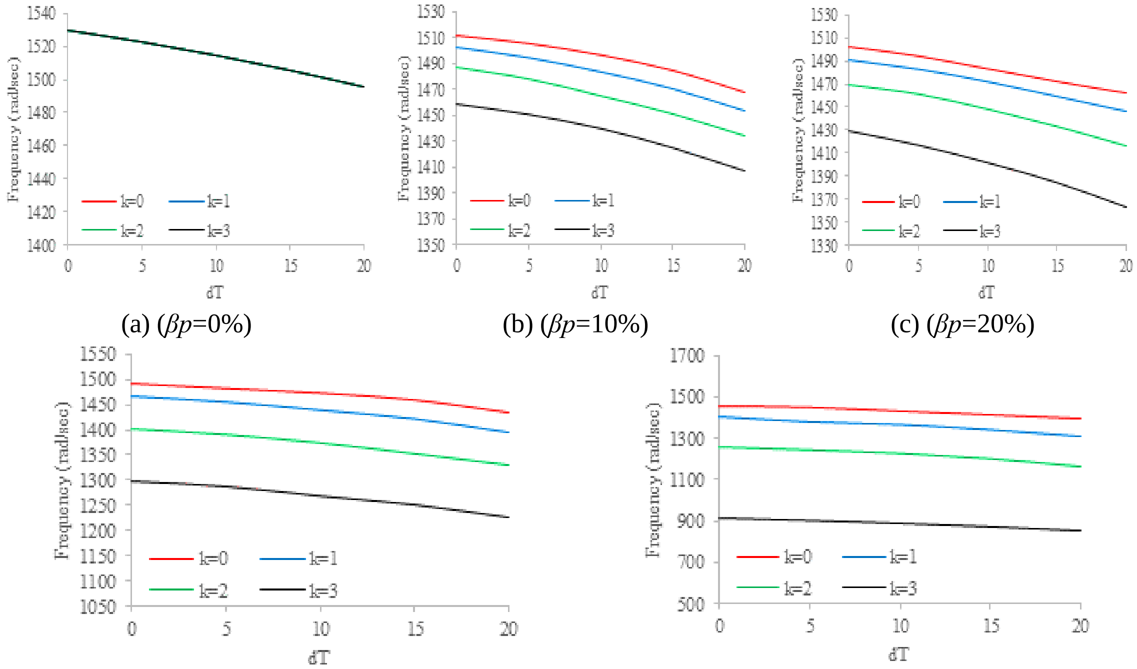

(a) (βp=0%) (b) (βp=10%) (c) (βp=20%)

(d) (βp=30%) (e) (βp=40%)

Fig. 8 Natural frequency of plate with FGM effect, for *dc*=20%

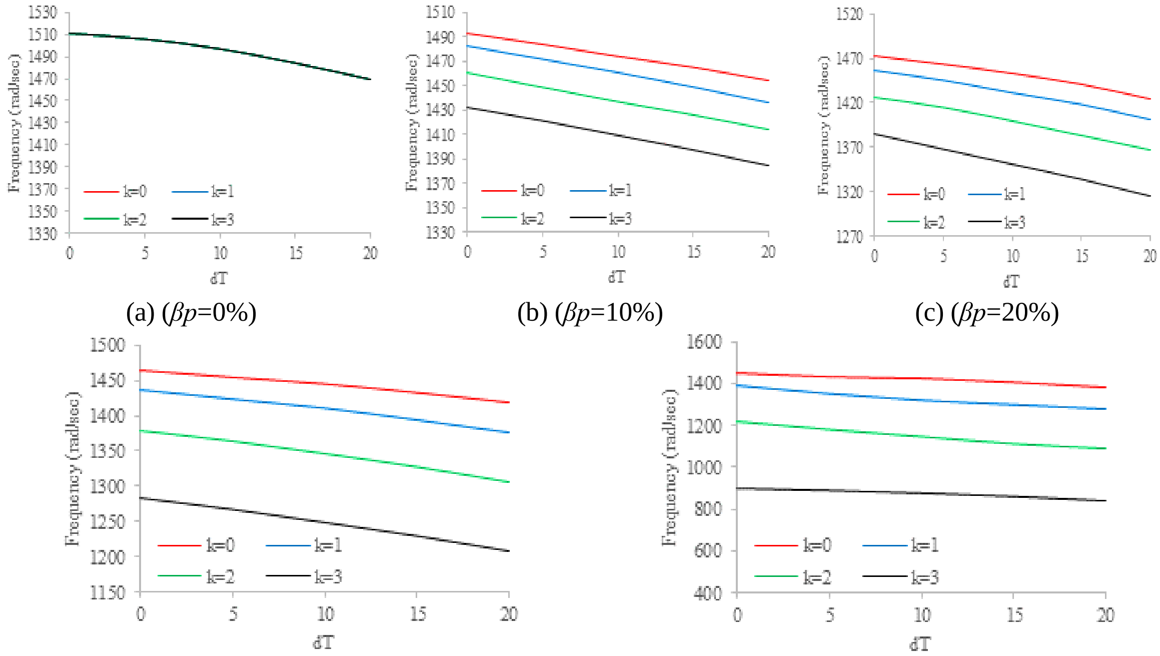

(a) (βp=0%) (b) (βp=10%) (c) (βp=20%)

(d) (βp=30%) (e) (βp=40%)

Fig. 9 Natural frequency of plate with FGM effect, for *dc*=30%

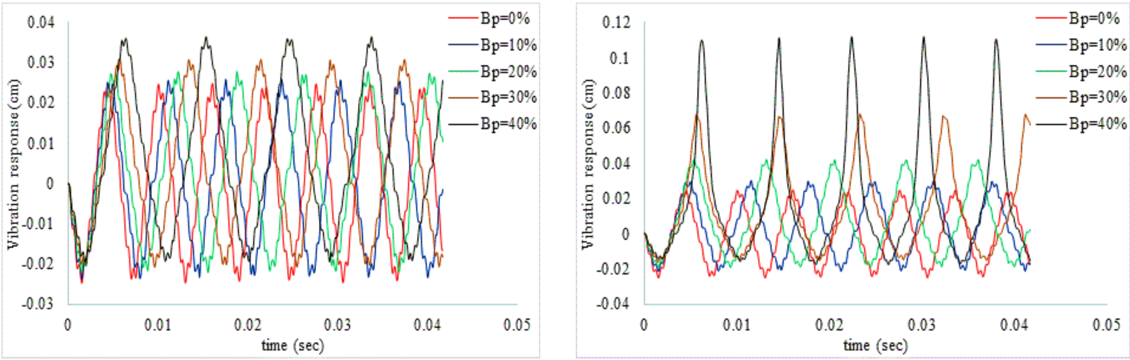

(a) (k =1) (b) (k =3)

Fig. 10 Vibration response of plate with porosity material effect for $dc = 0\%$ and $dT = 0$

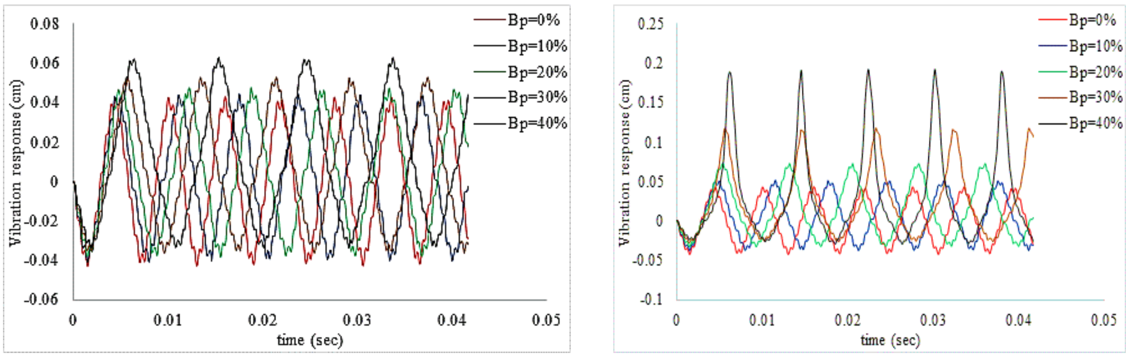

(a) (k =1) (b) (k =3)

Fig. 11 Vibration response of plate with porosity material effect for $dc = 30\%$ and $dT = 0$

change in the temperature difference ranging from (0 to 20)°C. Then, the calculation process was repeated for the same conditions, but with a power-law index (k) as unity.

The analysis was repeated for the same conditions by changing the parameters k as 2 and 3. It was found that the natural frequency and response were not affected. Further, for (βp=10%, dc=0%, k=0 to 3, dT=0 to 20°C), here, the natural frequency and response of the materials were examined and determined at the value of the difference in humidity (dc=0%) and a functional gradient (k=0) with a change in the temperature difference ranging from 0 to 20°C. The percentage of porosity was increased by 10%. Then, the calculation process was repeated for the same conditions, but with a functional gradient (k=1). Then the examination process was repeated for the same conditions at (k=2) and (k=3). It was noted that there was a small decrease in the natural frequency, accompanied by a slight increase. The response is due to the effect of increasing the porosity by 10% and the functional gradient with temperature change on the functionally graded materials, as in Fig. 6. The result of natural frequency shows that the porosity of materials led to a decrease in the natural frequency of the plate. It can be seen that the amount of decrease in the natural frequency at the value of the porosity ratio (βp=10%) is about 2%, while the amount of decrease in the natural frequency at the value of the porosity percentage βp=40%, reaches to 40%. A variation in functional gradient decreases the natural frequency with an increase in the response by a small amount.

5.3 Response results

The natural frequency of a PLA material was analyzed and the effect of porosity change on the functionally graded materials was studied, for the difference in humidity and the functional gradient (*dT*=0°C, *dc*=0%, *k*=1 to 3) as shown in Fig. 10. There was an increase in the magnitude of response when the functional gradient (*k*) was increased from *k*=1 to *k*=3. A higher magnitude is a result of high porosity in a material. It can be seen that the resulting response at the value of the porosity ratio of 40% was significantly greater than the resulting response at the value of 30%, 20%, and 10% porosity.

The response process was recalculated when the humidity was increased to 30% for functionally graded materials as shown in Fig. 11. Comparing the response magnitude for different dc values, a higher magnitude was seen for *dc*=30 % compared to *dc*=0%. From the results, it can be concluded that PLA material is sensitive to environmental factors such as temperature and humidity, so structures must be designed to accommodate these effects, especially in variable environments.

6. Conclusions

In this work, the authors investigated the nonlinear free vibration of porous functionally graded (PFG) plates under the influence of humidity changes. The fundamental natural frequency of PFG plates was computed for different parameters including porosity percentage, gradient index, and environmental properties. The adverse impacts of porosity can be significantly minimized by using appropriate values for stated factors. The natural frequency results of analytical and numerical methods were compared and found to be in good agreement where the maximum discrepancy between both techniques did not exceed 11%. The natural frequency results show that the drop in frequency is a peak value when the porosity, graduation, humidity, and temperature change have maximum value. In dynamic analysis, single-phase porous polymeric sandwich plates under hydrothermal conditions pose several challenges and limitations, including the degradation of materials by temperature and moisture, the porosity's complexity, and the materials' nonlinear behaviour. Additionally, imperfections at the interfaces between layers can affect dynamic stability. These limitations must be addressed in design and analysis to ensure that such materials are reliable and perform well in practical applications. The future direction includes the importance of optimizing material gradation and porosity to achieve the desired performance under dynamic loading and environmental conditions. By selecting appropriate porosity distributions and material gradation, the impact of hygrothermal changes can be mitigated to ensure the reliable performance of plate structure.

References

Abd Alqader, S.Q., Bedaiwi, B.O., Njim, E.K., Takhakh, A.M. and Hadji, L. (2024), "Free vibration analysis for polyester/graphene nanocomposites multilayer functionally graded plates", *Phys. Chem. Solid State*, **25**(4), 704-717. https://doi.org/10.15330/pcss.25.4.704-717.

Ali, A.Y. and Hasan, H.M. (2022), "Non-linear large amplitude vibration of orthotropic FGM convex and concave toroidal shell segments including the damping effect using the shear deformation theory", *Thin*

Wall. Struct., **173**, 109035. https://doi.org/10.1016/j.tws.2022.109035.

Allam, M.N.M., Radwan, A.F. and Sobhy, M. (2022), "Hygrothermal deformation of spinning FG graphene sandwich cylindrical shells having an auxetic core", *Eng. Struct.*, **251**, 113433. https://doi.org/10.1016/j.engstruct.2021.113433.

Avcar, M. (2019), "Free vibration of imperfect sigmoid and power law functionally graded beams", *Steel Compos. Struct.*, **30**(6), 603-615. https://doi.org/10.12989/scs.2019.30.6.603.

Avcar, M., Hadji, L. and Akan, R. (2022), "The influence of Winkler-Pasternak elastic foundations on the natural frequencies of imperfect functionally graded sandwich beams", *Geomech. Eng.*, **31**(1), 99-112. https://doi.org/10.12989/gae.2022.31.1.099.

Brischetto, S. and Torre, R. (2022), "3D hygro-elastic shell model for the analysis of composite and sandwich structures", *Compos. Struct.*, **285**, 115162. https://doi.org/10.1016/j.compstruct.2021.115162.

Foroutan, K., Carrera, E. and Ahmadi, H. (2021a), "Nonlinear hygrothermal vibration and buckling analysis of imperfect FG-CNTRC cylindrical panels embedded in viscoelastic foundations", *Eur. J. Mech.-A/Solid.*, **85**, 104107. https://doi.org/10.1016/j.euromechsol.2020.104107.

Foroutan, K., Carrera, E. and Ahmadi, H. (2021b), "Static and dynamic hygrothermal postbuckling analysis of sandwich cylindrical panels with an FG-CNTRC core surrounded by nonlinear viscoelastic foundations", *Compos. Struct.*, **259**, 113214. https://doi.org/10.1016/j.compstruct.2020.113214.

Garg, A., Belarbi, M.O., Chalak, H.D. and Chakrabarti, A. (2021), "A review of the analysis of sandwich FGM structures", *Compos. Struct.*, **258**, 113427. https://doi.org/10.1016/j.compstruct.2020.113427.

Ghazwani, M.H., Alnujaie, A., Avcar, M. and Van Vinh, P. (2024), "Examination of the high-frequency behavior of functionally graded porous nanobeams using nonlocal simple higher-order shear deformation theory", *Acta Mechanica*, **235**(5), 2695-2714. https://doi.org/10.1007/s00707-024-03858-6.

Gupta, A., Verma, S. and Ghosh, A. (2022), "Static and dynamic NURBS-based isogeometric analysis of composite plates under hygrothermal environment", *Compos. Struct.*, **284**, 115083. https://doi.org/10.1016/j.compstruct.2021.115083.

Hadji, L. and Avcar, M. (2020), "Free vibration analysis of FG porous sandwich plates under various boundary conditions", *J. Appl. Comput. Mech.*, **7**(2), 505-519. https://doi.org/10.22055/jacm.2020.35328.2628.

Hadji, L., Avcar, M. and Zouatnia, N. (2022), "Natural frequency analysis of imperfect FG sandwich plates resting on Winkler-Pasternak foundation", *Mater. Today: Proc.*, **53**, 153-160. https://doi.org/10.1016/j.matpr.2021.12.485.

He, Q., Dai, H.L., Zhang, Z. and Tang, H. (2022), "Hygro-thermo-elastic behavior for stiffened metal doubly-curved shallow shells with porous microcapsule coating under low-velocity impact considering in-plane initial load", *Compos. Struct.*, **284**, 115213. https://doi.org/10.1016/j.compstruct.2022.115213.

Hellal, H., Bourada, M., Hebali, H., Bourada, F., Tounsi, A., Bousahla, A.A. and Mahmoud, S. (2021), "Dynamic and stability analysis of functionally graded material sandwich plates in hygro-thermal environment using a simple higher shear deformation theory", *J. Sandw. Struct. Mater.*, **23**(3), 814-851. https://doi.org/10.1177/1099636219845841.

Hu, J., Jin, J., Xuan, S., Mi, S., Tian, W. and Liao, W. (2022), "Influence of cyclical hygrothermal aging on mechanical response and structural durability of composite bolted interference-fit joints", *Thin Wall. Struct.*, **173**, 108997. https://doi.org/10.1016/j.tws.2022.108997.

Hua, F., Fu, W. and Zhou, X. (2022), "Wave propagation analysis of sandwich plates with graphite particles filled viscoelastic material core in hygrothermal environments", *Compos. Struct.*, **288**, 115380. https://doi.org/10.1016/j.compstruct.2022.115380.

Karimiasl, M. and Alibeigloo, A. (2022), "Nonlinear free and forced vibration analysis of sandwich cylindrical panel with auxetic core and GPLRC facing sheets in hygrothermal environment", *Thin Wall. Struct.*, **175**, 109164. https://doi.org/10.1016/j.tws.2022.109164.

Kiarasi, F., Babaei, M., Asemi, K., Dimitri, R. and Tornabene, F. (2022), "Free vibration analysis of thick annular functionally graded plate integrated with Piezo-Magneto-Electro-Elastic layers in a hygrothermal environment", *Appl. Sci.*, **12**(20). https://doi.org/10.3390/app122010682.

Madan, R., Khobragade, P., Mussada, E.K., Singh, M.K., Rangappa, S.M., Njim, E.K. and Siengchin, S.

(2025), "A novel two-step finite element approach to estimate the thermo-mechanical properties of two-phase and three-phase hybrid composites", *Compos. Commun.*, **53**, 102213. https://doi.org/10.1016/j.coco.2024.102213.

Monge, J.C., Mantari, J.L. and Arciniega, R.A. (2022), "3D semi-analytical solution of hygro-thermo-mechanical multilayered doubly-curved shells", *Eng. Struct.*, **256**, 113916. https://doi.org/10.1016/j.engstruct.2022.113916.

Mouthanna, A., Bakhy, S.H., Al-Waily, M. and Njim, E.K. (2024), "Free vibration investigation of single-phase porous FG sandwich cylindrical shells: Analytical, numerical and experimental study", *Iran. J. Sci. Technol., Trans. Mech. Eng.*, **48**(3), 1135-1159. https://doi.org/10.1007/s40997-023-00700-7.

Njim, E.K., Almamuri, M.H., Bakhy, S.H., Idan, Z.S., Al-Waily, M., Jweeg, M.J. and Hadji, L. (2024), "Experimental and numerical analysis of uni-axial buckling of single-phase functionally graded porous polymeric sandwich plates", *BIO Web Conf.*, **97**, 00002. https://doi.org/10.1051/bioconf/20249700002.

Njim, E.K., Bakhy, S.H. and Al-Waily, M. (2021), "Free vibration analysis of imperfect functionally graded sandwich plates: Analytical and experimental investigation", *Arch. Mater. Sci. Eng.*, **111**(2), 49-65. https://doi.org/10.5604/01.3001.0015.5805.

Njim, E.K., Bakhy, S.H. and Al-Waily, M. (2022), "Experimental and numerical flexural analysis of porous functionally graded beams reinforced by (Al/Al2O3) nanoparticles", *Int. J. Nanoelectron. Mater.*, **15**(2), 91-106.

Parhi, A., Singh, B.N. and Panda, S.K. (2021), "Nonlinear free vibration analysis of composite conical shell panel with cluster of delamination in hygrothermal environment", *Eng. Comput.*, **37**(2), 1565-1577. https://doi.org/10.1007/s00366-019-00903-0.

Raad, H., Najim, E., Jweeg, M., AlWaily, M., Hadji, L. and Madan, R. (2024), "Vibration analysis of sandwich plates with hybrid composite cores combining porous polymer and foam structures", *J. Comput. Appl. Mech.*, **55**(3). https://doi.org/10.22059/jcamech.2024.377658.1121.

Rubine, L., Selvamani, R. and Ebrahimi, F. (2024), "Nonlinear thermal vibration of fluid infiltrated magneto piezo electric variable nonlocal FG nanobeam with voids", *Couple. Syst. Mech.*, **13**(4), 337-357. https://doi.org/10.12989/csm.2024.13.4.337.

Sabherwal, P., Belarbi, M.O., Raman, R., Garg, A., Li, L., Devidas Chalak, H., Ahmed Houari, M.S. and Avcar, M. (2024), "Free vibration analysis of laminated sandwich plates using wavelet finite element method", *AIAA J.*, **62**(2), 824-832. https://doi.org/10.2514/1.j063364.

Sobhy, M. (2021), "3-D elasticity numerical solution for magneto-hygrothermal bending of FG graphene/metal circular and annular plates on an elastic medium", *Eur. J. Mech.-A/Solid.*, **88**, 104265. https://doi.org/10.1016/j.euromechsol.2021.104265.

Tang, H. and Dai, H.L. (2021a), "Dynamic instability zone analysis of laminated piezoelectric cylindrical shell with delamination under hygrothermal effects", *Appl. Math. Model.*, **99**, 27-40. https://doi.org/10.1016/j.apm.2021.04.014.

Tang, H. and Dai, H.L. (2021b), "Nonlinear vibration behavior of CNTRC plate with different distribution of CNTs under hygrothermal effects", *Aerosp. Sci. Technol.*, **115**, 106767. https://doi.org/10.1016/j.ast.2021.106767.

Tang, H. and Dai, H.L. (2021c), "Nonlinear vibration analysis of CFRP spherical shell panel under hygrothermal effects", *Compos. Struct.*, **274**, 114343. https://doi.org/10.1016/j.compstruct.2021.114343.

Tayeb, B., Abderezak, R. and Daouadji, T.H. (2024), "Mechanical behavior of composite beam aluminum-sandwich honeycomb strengthened by imperfect FGM plate under thermo-mechanical loading", *Couple. Syst. Mech.*, **13**(2), 133-151. https://doi.org/10.12989/csm.2024.13.2.133.

Wang, S., Kang, W., Yang, W., Zhang, Z., Li, Q., Liu, M. and Wang, X. (2022), "Hygrothermal effects on buckling behaviors of porous bi-directional functionally graded micro-/nanobeams using two-phase local/nonlocal strain gradient theory", *Eur. J. Mech.-A/Solid.*, **94**, 104554. https://doi.org/10.1016/j.euromechsol.2022.104554.

Zaidan, S.M. and Hasan, H.M. (2022), "Parametric Instability of functionally graded porous cylindrical panels under the effect of static and time-dependent axial loads", *Vib.*, **5**(3), 570-584. https://doi.org/10.3390/vibration5030033.

Zaitoun, M.W., Chikh, A., Tounsi, A., Al-Osta, M.A., Sharif, A., Al-Dulaijan, S.U. and Al-Zahrani, M.M. (2022), “Influence of the visco-Pasternak foundation parameters on the buckling behavior of a sandwich functional graded ceramic-metal plate in a hygrothermal environment”, *Thin Wall. Struct*., **170**, 108549. https://doi.org/10.1016/j.tws.2021.108549.

Zenkour, A.M. and El-Shahrany, H.D. (2020), “Hygrothermal effect on vibration of magnetostrictive viscoelastic sandwich plates supported by Pasternak’s foundations”, *Thin Wall. Struct.*, **157**, 107007. https://doi.org/10.1016/j.tws.2020.107007.

Zenkour, A.M. and El-Shahrany, H.D. (2021), “Hygrothermal vibration of adaptive composite magnetostrictive laminates supported by elastic substrate medium”, *Eur. J. Mech.-A/Solid.*, **85**, 104140. https://doi.org/10.1016/j.euromechsol.2020.104140.

Zhao, J., Hu, J., Wang, T., Li, H., Guan, J., Liu, J. and Gao, Z. (2022), “A unified modeling method for dynamic analysis of GPLs-FGP sandwich shallow shell embedded SMA wires with general boundary conditions under hygrothermal loading”, *Eng. Struct.*, **250**, 113439. https://doi.org/10.1016/j.engstruct.2021.113439.

Zohra, A., Rabia, B. and Tahar, H.D. (2024), “Study and analysis of porosity distribution effects on the buckling behavior of functionally graded plates subjected to diverse thermal loading”, *Couple. Syst. Mech.*, **13**(2), 115-132. https://doi.org/10.12989/csm.2024.13.2.115.

Zouatnia, N., Hadji, L., Atmane, H.A., Nebab, M., Madan, R., Bennai, R. and Dahmane, M. (2024), “Analysis of free vibration in bi-directional power law-based FG beams employing RSD theory”, *Couple. Syst. Mech.*, **13**(4), 359-373. https://doi.org/10.12989/csm.2024.13.4.359.

Appendix

$$r_{12} = -K_s I_{30}\lambda_m, r_{13} = -K_s I_{30}\delta_n, r_{14} = (H_{12} + H_{13}) - \frac{H_{25}H_{27}}{H_{26}} - \frac{H_{27}H_{29}}{H_{26}},$$

$$r_{15} = (H_{14} + H_{15}) - \frac{H_{25}H_{28}}{H_{26}} - \frac{H_{28}H_{29}}{H_{26}}, r_{16} = (H_{23} + H_{24})\Phi_1 + (H_{33} + H_{34})\Phi_2 - K_s I_{30}\lambda_m^2 - K_s I_{30}\delta_n^2,$$

$$r_{17} = (H_{16} + H_{17}) - H_{31}, r_{18} = (H_{16} + H_{17}) - 2H_{31}, r_{19} = -(H_{18} + H_{19}) - \frac{1}{16}\left(\frac{\lambda_m^2}{A_{22}} + \frac{\delta_n^2}{A_{11}}\right),$$

$$r_{110} = -(H_{18} + H_{19}) - (H_{21} + H_{22}) - \frac{3}{16}\left(\frac{\lambda_m^4}{A_{22}} + \frac{\delta_n^4}{A_{11}}\right), r_{111} = -(H_{21} + H_{22}) - \frac{1}{8}\left(\frac{\lambda_m^4}{A_{22}} + \frac{\delta_n^4}{A_{11}}\right),$$

$$r_{21} = 0, r_{22} = -D_{11}\lambda_m^2 - D_{66}\delta_n^2 - K_s I_{30} - B_{21}\frac{\zeta}{S}\lambda_m^3 - (B_{11} - B_{66})\frac{\zeta}{S}\lambda_m\delta_n^2,$$

$$r_{23} = -(D_{12} + D_{66})\lambda_m\delta_n - B_{21}\frac{\Psi}{S}\lambda_m^3 - (B_{11} - B_{66})\frac{\Psi}{S}\lambda_m\delta_n^2, r_{31} = 0,$$

$$r_{32} = -(D_{21} + D_{66})\lambda_m\delta_n - B_{12}\frac{\zeta}{S}\delta_n^3 - (B_{22} - B_{66})\frac{\zeta}{S}\lambda_m^2\delta_n,$$

$$r_{33} = -D_{22}\delta_n^2 - D_{66}\lambda_m^2 - K_s I_{30} - B_{12}\frac{\Psi}{S}\delta_n^3 - (B_{22} - B_{66})\frac{\Psi}{S}\lambda_m^2\delta_n, n_7 = -K_s I_{30}\lambda_m, n_8 = -\frac{8}{3}\frac{B_{21}}{A_{11}}\frac{\delta_n}{ab},$$

$$n_9 = -K_s I_{30}\delta_n, n_{10} = -\frac{8}{3}\frac{B_{12}}{A_{22}}\frac{\lambda_m}{ab}, \tilde{\rho}_1 = \left(I_2 - \frac{I_1^2}{I_0}\right), H_{11} = (A_{11}A_{22} - A_{12}^2),$$

$$H_{12} = \frac{4\lambda_m^2(B_{21}A_{12} + A_{11}B_{11})}{\delta_n abH_{11}}, H_{13} = \frac{4\delta_n(B_{11}A_{12} + A_{11}A_{22}B_{21})}{abH_{11}}, H_{14} = \frac{4\lambda_m(B_{22}A_{12} + A_{11}B_{12})}{abH_{11}},$$

$$H_{15} = \frac{4\delta_n^2(B_{12}A_{12} + A_{22}B_{22})}{\lambda_m abH_{11}}, H_{16} = 0, H_{17} = 0, H_{18} = \frac{\lambda_m^3\delta_n(\delta_n^2A_{12} + \lambda_m^2A_{22})}{8abH_{11}},$$

$$H_{19} = \frac{\delta_n^3\lambda_m(\lambda_m^2A_{12} + \delta_n^2A_{22})}{8abH_{11}}, H_{21} = \frac{\lambda_m^3\delta_n(\delta_n^2A_{12} + \lambda_m^2A_{11})}{4abH_{11}}, H_{22} = \frac{\lambda_m\delta_n^3(\lambda_m^2A_{12} + \delta_n^2A_{22})}{4abH_{11}},$$

$$H_{23} = \frac{\lambda_m^2(C_{11}^*A_{11} + C_{22}^*A_{12})}{H_{11}}, H_{24} = \frac{\delta_n^2(C_{11}^*A_{12} + C_{22}^*A_{22})}{H_{11}}, H_{25} = \frac{8\lambda_m\delta_n}{ab},$$

$$H_{26} = A_{11}\lambda_m^4 + A_{22}\delta_n^4 + (A_{66} - 2A_{12})\lambda_m^2\delta_n^2, H_{27} = B_{21}\lambda_m^3 + (B_{11} - B_{66})\lambda_m\delta_n^2,$$

$$H_{28} = B_{12}\delta_n^3 + (B_{22} - B_{66})\lambda_m^2\delta_n, H_{29} = \frac{16\lambda_m^2\delta_n^2}{3mn\pi^2}, H_{31} = 0, H_{32} = \frac{16}{mn\pi^2}, H_{33} = \frac{\lambda_m^2(A_{11} + A_{12})}{H_{11}},$$

$$H_{34} = \frac{\delta_n^2(A_{12} + A_{22})}{H_{11}}, \zeta = B_{21}\lambda_m^3 + (B_{11} - B_{66})\lambda_m\delta_n^2, \Psi = B_{12}\delta_n^3 + (B_{22} - B_{66})\lambda_m^2\delta_n,$$

$$S = A_{11}\lambda_m^4 + A_{22}\delta_n^4 + (A_{66} - 2A_{12})\lambda_m^2\delta_n^2,$$